JOURNAL OF GEOPHYSICAL RESEARCH, VOL. 104, NO. D21, PAGES 26,209-26,218, NOVEMBER 20, 1999

Assimilation of Measurement of Air Pollution from Space (MAPS) CO in a global three-dimensional model

J.-F. Lamarque, B. V. Khattatov, J. C. Gille, and G. P. Brasseur

Atmospheric Chemistry Division, National Center for Atmospheric Research, Boulder, Colorado

Abstract. Observations of carbon monoxide (CO) by the Measurement of Air Pollution from Space (MAPS) instrument onboard the space shuttle were assimilated into a global three-dimensional chemistry-transport model using the Physical-space Statistical Analysis System approach. The assimilation considerably improved the calculated distribution of CO in the troposphere. On the global scale, the adjustment of the CO field resulting from the assimilation procedure was large at the beginning of the assimilation, suggesting discrepancies in the initial conditions of the model. As the model integration/assimilation progressed with time, transport caused the model to drift. This drift limited to a few days the "memory" of CO from its adjustment toward the observations. The assimilation of CO significantly influenced the distribution of other chemical species, even over the limited time periods (~ 10 days) analyzed.

1. Introduction

Knowledge of the global distribution of carbon monoxide (CO) in the troposphere is important to assess the chemical state of the global troposphere. Indeed, in the free troposphere, the reaction of CO with the hydroxyl radical (OH) provides the major sink of OH and hence influences the oxidizing capacity of the atmosphere [*Levy*, 1971]. Furthermore, in the presence of sufficiently large amounts of nitrogen oxides, the reaction with OH can lead to a net production of ozone [*Crutzen*, 1973]. In the troposphere, carbon monoxide is emitted as a result of incomplete biomass and fossil fuel combustion processes. CO is also a product of the oxidation of methane and nonmethane hydrocarbons. The anthropogenic source of CO is expected to rise over the next decades, particularly over southeastern Asia due to increased economic activity and growing population. Despite its considerable importance, the distributions of CO concentrations and of CO sources are not well known and consequently model simulations are subject to large uncertainties. Recent modeling studies have clearly highlighted some deficiencies in the simulation of the observed CO distribution [*Allen et al.*, 1996; *Berntsen and Isaksen*, 1997; *Chatfield et al.*, 1998; *Hauglustaine et al.*, 1998].

Data assimilation incorporates observations into model simulations, resulting in improved distributions of specific quantities. Unlike observations, which are related to a specific field measured at a specific time and location, data assimilation methods provide a four-dimensional (time and space) description of the dynamical and chemical state of the atmosphere [*Errico*, 1999]. The assimilation procedure determines the distribution of a specific field that minimizes a measure of the distance (usually in a least squares sense) between the calculated and observed distributions of the same field [*Talagrand*, 1997; *Errico*, 1999]. This distance is formulated using weights that depend on the respective error distributions. Under some simplifying assumptions [e.g., *Cohn*, 1997], the Kalman-Bucy filter provides a solution to this minimization problem. The Kalman-Bucy filter can also dynamically estimate covariances of the forecast error [*Talagrand*, 1997]. For global problems in atmospheric sciences, this approach is not yet computationally feasible. For that reason, simplified versions of the Kalman-Bucy filter have been designed. In particular, we use a simplification of the Kalman-Bucy filter in which the forecast error covariance is prescribed. This method is similar to the Physical-space Statistical Analysis System (PSAS) [*Da Silva et al.*, 1995].

For the assimilation to be most effective at the global scale, a data set with frequent extensive coverage is necessary. At the present time, the only CO data set with such characteristics is provided by the Measurement of Air Pollution from Space (MAPS) campaign. The MAPS instrument flew onboard the space shuttle in November 1981 and October 1984. Following these experimental flights, two more flights were performed in April (April 9 to 19) and October (September 30 to October 11) of 1994. The data from these last two campaigns are used in this study as the observations to be assimilated.

The goal of this paper is to investigate the impact of assimilating CO on tropospheric chemistry. For that purpose, we use a global three-dimensional chemistry-transport model (CTM) into which the MAPS observations are assimilated using the PSAS approach. The observations and modeling tools are described in sections 2 and 3. In section 4, after a model-data comparison, we discuss the impact of the assimilation on the calculated CO distribution. Specifically, we assess the role of transport and chemistry in the evolution of the discrepancy between model and observations. Finally, we analyze the impact of assimilation on chemical species other than CO.

2. Data Description

The available MAPS data cover two distinct periods. The data were produced by the NASA Langley Research Center, Atmospheric Sciences Division. The April data are from the Space Radar Laboratory (SRL-1) on the space shuttle flight STS-59, and the October data are from the Space Radar Laboratory (SRL-2) on the space shuttle flight STS-68 [*Reichle et al.*, 1990;

Paper number 1999JD900807.
0148-0227/99/1999JD900807$09.00

Connors et al., 1996]. The contribution of the CO distribution at different altitudes to the overall radiometric signal is provided by the convolution of the vertical CO distribution with the instrumental signal function [*Reichle et al.*, 1999, hereinafter R99]. As a consequence, at a given geographical location, a MAPS observation consists of a single value, which is the integrated value of CO weighted by the signal function. It is important to note that the signal function goes to zero at the ground, indicating that the signal recorded by the instrument contains no information on the CO concentration in the boundary layer. The reader is referred to R99 for the description of the signal function.

The MAPS instrument collected data every second, with an instantaneous square field of view of 17×17 km^2 along the track of the space shuttle (R99). An extensive latitudinal and longitudinal coverage is achieved every 12 hours. Validation against aircraft-borne direct measurements can be found in R99. Such comparison indicates that the MAPS data, when interpreted as a total column, are within ~ 10% of the values measured by the aircraft. The data are available in two forms: gridded and ungridded. The ungridded data are unfiltered and might be contaminated by extreme values due to the presence of clouds at the location of the observation. To alleviate this problem, a filter based on the N_2O distribution measured simultaneously was designed (R99). The gridded data are a subset of the ungridded data, filtered for clouds, averaged over a 1-day period, and binned at a 5° horizontal resolution. To provide the highest possible time resolution, we have used the ungridded data, with the same cloud filtering for the observations as in R99.

3. Model Description

This section describes the two principal modules of the model used in this study: the chemistry-transport module and the assimilation module.

3.1. Chemistry-Transport Module

We used an updated version of the global tropospheric chemistry-transport model (CTM) called MOZART (Model for OZone And Related chemical Tracers), recently developed at the National Center for Atmospheric Research (NCAR) [*Mahowald et al.*, 1997; *Rasch et al.*, 1997; *Brasseur et al.*, 1998; *Hauglustaine et al.*, 1998]. We describe only the characteristics of the model relevant to the present study. For a complete description of the model and its evaluation, the reader is referred to *Brasseur et al.* [1998] and *Hauglustaine et al.* [1998], respectively.

In its standard version, MOZART provides the distribution of 56 chemical constituents between the surface and the upper stratosphere, at a horizontal resolution (T42) of ~ 2.8° in both latitude and longitude. The continuity equations for these species are solved and account for advection, convection, and diffusive transport, as well as surface emissions, photochemical conversions, and wet and dry deposition. The evolution of species due to all physical and chemical processes is calculated with a timestep of 20 min.

For this study, we updated the MOZART model to use analyzed winds provided by the National Centers for Environmental Prediction (NCEP). The vertical discretization consists of 28 σ-levels from the ground to ~ 5 mbar. In order to save computer time and memory, the horizontal resolution was degraded to T21, i.e., ~ 5.6° in both latitude and longitude. Furthermore, the chemical scheme was simplified and neglects the reactions associated with nonmethane hydrocarbons. The assumption behind this simplification of the chemical scheme is that it will not affect significantly the simulation of the CO distribution over the 2-week period considered, while being much less computationally expensive. We will discuss the influence of this latter simplification later in this paper (see section 4.5).

3.2. Assimilation Module

As mentioned previously, each MAPS observation consists of a vertically integrated average of the tropospheric CO profile. Since the chemistry-transport model did not explicitly compute such a variable, we needed to transform a model CO profile into the value that MAPS would observe under such conditions. For that purpose, we used the averaging kernel formulation from R99. The equivalent MAPS value was calculated as the convolution of the CO profile with the averaging kernel. The shape of the averaging kernel is shown in Figure 1.

The assimilation procedure requires the definition of an observation operator that transforms the values from the model space (a CO vertical profile in a model grid column) to the observation space (a tropospheric weighted average at the location of the MAPS observation). In our case, this observation operator consists of a horizontal interpolation to the location of the observation followed by the convolution of the horizontally interpolated CO profile with the averaging kernel (see Figure 1). This operator is therefore linear.

For a linear observation operator, the central equation to data assimilation, known as the Optimal Interpolation equation [*Lorenc*, 1986], is given by

$$\delta \mathbf{x}^a = \mathbf{K}(\mathbf{x}^{obs} - \mathbf{H}\mathbf{x}^b), \qquad (1)$$

where $\delta \mathbf{x}^a$ is the analysis increment, which, when added to the background $\mathbf{x}^b$, provides the analyzed field $\mathbf{x}^a$ [*Courtier et al.*, 1998]. In our case, the model simulations are considered to be the a priori background estimate. The term background will

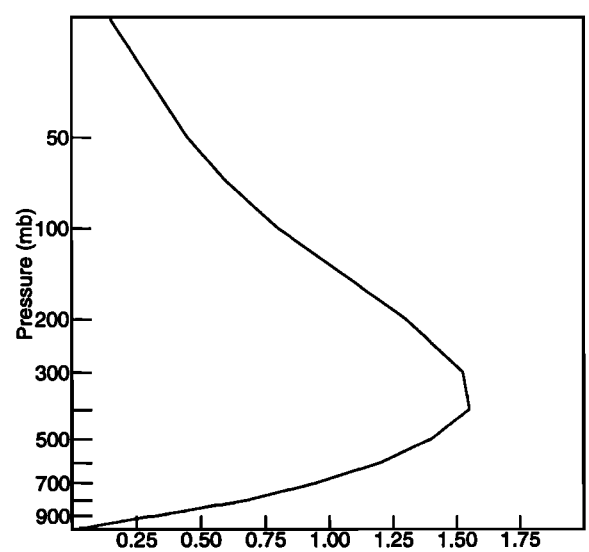

Figure 1. Averaging kernel for the MAPS CO channel. Adapted from *Reichle et al.* [1999].

therefore refer to the model field for the rest of this paper. **H** is a matrix representation of the linear observation operator, and $\mathbf{x}^{obs}$ are the observations.

The Kalman gain matrix **K** is expressed as

$$\mathbf{K} = \mathbf{B}\mathbf{H}^t(\mathbf{H}\mathbf{B}\mathbf{H}^t + \mathbf{R})^{-1}, \quad (2)$$

where **B** is the covariance matrix of the background (i.e., model) field errors and **R** is the covariance matrix of observation errors. $\mathbf{H}\mathbf{B}\mathbf{H}^t$ can be viewed as the matrix of the covariances of background errors in observation space, while $\mathbf{B}\mathbf{H}^t$ is the matrix of covariances between the background errors in model space and the background errors in observation space [*Courtier et al.*, 1998]. By calculating some or all of the covariance matrix elements in observation space, we reduced the order of matrices to be processed from the number of three-dimensional grid points in the model (typically 200,000 in the case of MOZART at the T42 resolution) to the number of observations (around 10,000 for a 12-hour period). To further reduce the order of the matrices, we aggregated in space all the observations located in the same model grid cell.

Following the PSAS approach [*Da Silva et al.*, 1995], (1) is rewritten as

$$(\mathbf{H}\mathbf{B}\mathbf{H}^t + \mathbf{R})\mathbf{w} = \mathbf{x}^{obs} - \mathbf{H}\mathbf{x}^b \quad (3)$$

$$\delta\mathbf{x}^a = \mathbf{B}\mathbf{H}^t\mathbf{w} \quad (4)$$

so that the solution **w** of the linear system (3) is a vector in the observation space, which in our case is much smaller than the model space. In our implementation, (3) is solved by LU-decomposition instead of a conjugate gradient method as of *Da Silva and Guo* [1996]. This procedure, along with other numerical specificities, are described by B. Khattatov et al. (manuscript in preparation, 1999).

In our study, the background error covariances are prescribed. This prescription has a profound influence on the vertical distribution of the analysis increment $\mathbf{x}^a$. The transformation of the difference in observation space ($(\mathbf{x}^{obs} - \mathbf{H}\mathbf{x}^b)$ in (1)) into the difference in physical space (i.e., the analysis increment) is achieved through the multiplication by the gain matrix **K**. A commonly used form of the covariance, in both the horizontal and vertical planes, is

$$\mathbf{B}(i,j) = \sigma(i)\,\sigma(j)\,\exp\left(-\frac{d_{xy}(i,j)^2}{2L_{xy}^2}\right)\exp\left(-\frac{d_z(i,j)^2}{2}\right), \quad (5)$$

where $\sigma(i)$ is the variance of the model CO at the location i, $d_{xy}(i,j)$ is the horizontal great-circle distance between points i and j, and $d_z(i,j)$ the vertical distance, expressed in units of scale height (1 scale height ~ 7 km). This form of $\mathbf{B}(i,j)$ means that the correlation model considered here is separable [*Gaspari and Cohn*, 1999]. L_{xy} is a preset correlation length taken as 1000 km. In practice, we use a compactly supported covariance function that approximates the Gaussian distribution [*Gaspari and Cohn*, 1999]. This compact support characteristic ensures that $\mathbf{B}(i,j)$ is explicitly 0 for horizontal distances $d_{xy}(i,j)$ larger than $2L_{xy}$ and/or vertical distances larger than 2 scale heights. As a consequence, the covariance matrix was sparser than if Gaussian functions were used, since those go to zero only at infinity. The background variance was calculated assuming a fixed 30% relative error on the model CO field, which is representative of the MOZART results discussed by *Hauglustaine et al.* [1998].

For the observation error covariance matrix **R**, we assumed the observation errors to be independent, a reasonable assumption for nadir-viewing instruments. The matrix **R** was therefore diagonal. From R99, the observational error standard deviation is set to a constant 20% relative error.

Because the space shuttle flight track begins to retrace its path after every 12 hours approximately, we performed the assimilation every 12 hours using the MAPS data collected over the previous 12 hours. This led to a discontinuity in the evolving CO field each time the assimilation was performed.

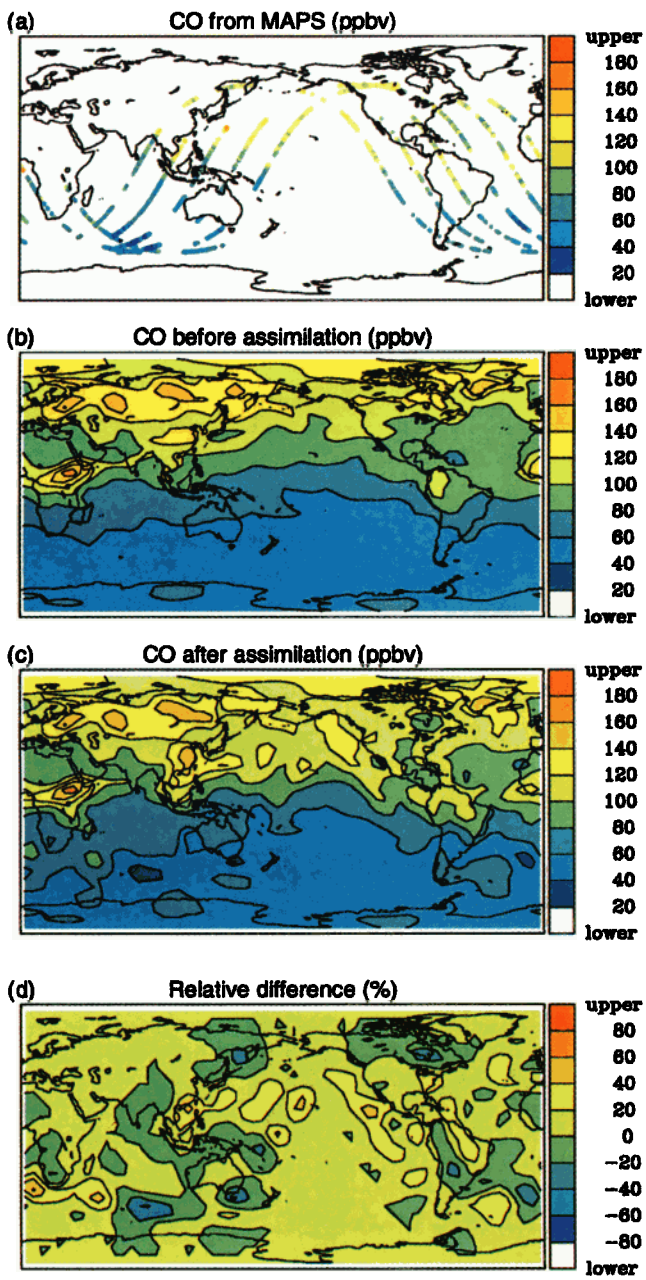

Plate 1. Latitude-longitude distribution of the weighted model CO (see text for details) on April 10, 0000 UT 1994. Units are ppbv. (a) Filtered observations from MAPS, accumulated over a 12-hour period. (b) Model results before the assimilation. (c) Model results after the assimilation of the data shown in Plate 1a. (d) Relative difference between the CO distribution after and before the assimilation (see text for details).

4. Assimilation Results

In this section we discuss the results from the assimilation of the MAPS observations of CO in the MOZART model for both the April and October 1994 periods. In all cases, we took the initial conditions for the chemical species from the standard MOZART simulation discussed by *Hauglustaine et al.* [1998], degraded to the T21 resolution and interpolated to the starting time of the simulation. It must be kept in mind that the original MOZART results were obtained using the winds generated by a climate model which are therefore different than the analyzed winds used in this study. As a consequence, the CO distribution used as initial conditions was different from the distribution that would have been obtained using analyzed winds. Nevertheless, it was found that the sensitivity of the model results to the initial conditions was small (see section 4.1). All simulations were run for the length of the observation periods.

4.1. Model-Data Comparison

Since the model assimilated the observed MAPS mixing ratios, it is natural to compare these observations to the value of the collocated model profile after vertical integration with the averaging kernel as weighting function (see section 3.2). For the remainder of this paper, we will call such a value weighted model CO.

Results from the assimilation of CO are shown in Plate 1 for April 10, 0000 UT. Since MAPS data are only available from April 9, 1200 UT, the first assimilation cycle performed on April 10, 0000 UT, used the data collected over the previous 12 hours. The results shown are qualitatively representative of the general behavior of the effect of the assimilation of CO for the whole period of study.

In Plate 1a, the accumulated observations of CO from MAPS, after cloud filtering, are displayed as they were taken along the space shuttle flight track. Plates 1b and 1c present the weighted model CO before and after assimilation, respectively. Before assimilation, although the model provides a reasonable simulation of the major features of CO, it clearly misrepresents some broad scale peaks seen in the MAPS data. After assimilation the general distribution of CO is in better agreement with the observations. In particular, the low values in the Southern Hemisphere and the high values over southeast Asia and Japan and off the west coast of the United States are captured only after the assimilation process was applied. These features are present even though the resolution of the model is relatively coarse (T21). The general improvement in the calculated CO distribution can be expected because the error in the observations was assigned to be smaller than the error in the model CO field. The horizontal spread of the adjustment of CO around the location of the observation is due to the shape of the background covariance function (equation (5)). In this study, each observation influenced the CO field over a circular area centered over the location of the observation, with a weight decreasing exponentially away from the point where the observation was made.

Plate 1d presents the relative difference

$$\frac{CO^{after} - CO^{before}}{CO^{before}}$$

where before and after refer to the application of the CO assimilation. At this point in the simulation, the modification of the weighted model CO from its assimilation is as large as ±50%. The implication of this modification to the CO distribution is studied in more detail in section 4.5.

As a measure of the misfit between the observations and the model results, the root-mean-square (RMS) error σ_m

$$\sigma_m = \sqrt{\frac{1}{N}\sum_{i=1}^{N}\left(y_i^{obs} - y_i^{model}\right)^2} \qquad (6)$$

is calculated, with N being the number of observations for the time period under consideration, y^{obs} are the MAPS observations, and y^{model} are the weighted model CO values from the model simulations, interpolated to the location of the observations. Figures 2a and 2b show the evolution of σ_m over the course of the assimilation period for the April and October cases, respectively. To measure the effect of the assimilation, the value of σ_m is shown before and after assimilation, performed every 12 hours of the model simulation. Though it is clear that the assimilation consistently improves the quality of the simulation, this improvement plateaus after only a few assimilation cycles. The value of σ_m for the CO distribution after assimilation is almost constant with time. This constancy is expected because the degree of improvement through assimilation is primarily limited by the relative error of the observations, which was defined as constant through time.

It is important to note that σ_m contains both the bias and the standard deviation. The bias δ_m is defined as

$$\delta_m = \frac{1}{N}\sum_{i=1}^{N}\left(y_i^{obs} - y_i^{model}\right). \qquad (7)$$

The time evolution of the bias, in both April and October cases, for the simulation with and without assimilation, is shown as Figures 3a and 3b. The bias after assimilation is quite small and negative in both cases. The bias is found to be large at the beginning of the October simulation, as expected from Figure 2b.

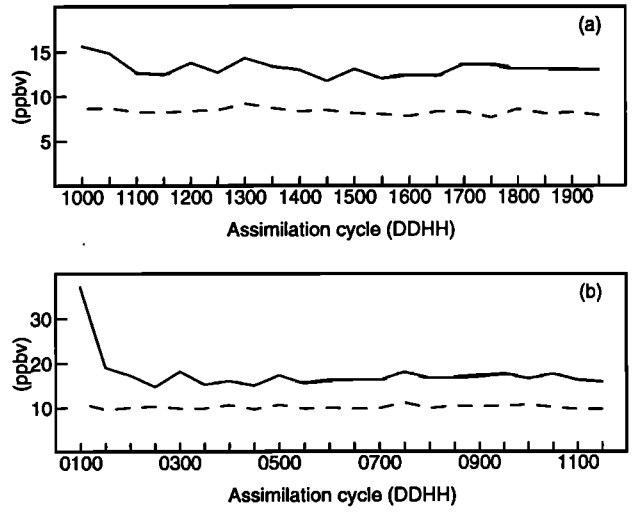

Figure 2. Time evolution of σ_m (see equation (6)) for the simulation before assimilation (solid line) and after assimilation (dashed line): (a) for the April campaign and (b) for the October campaign.

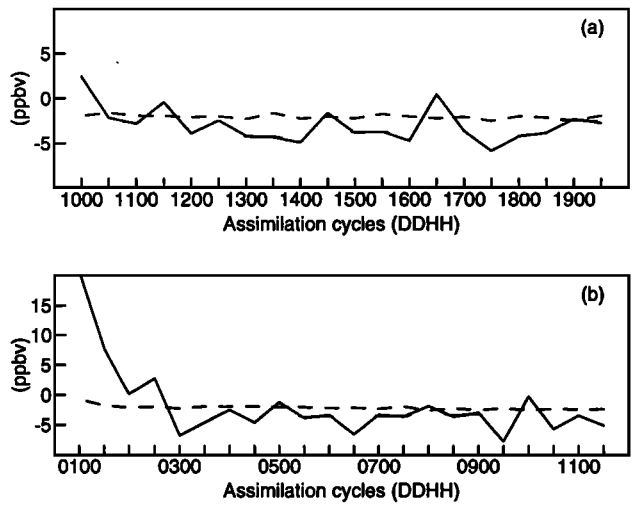

Figure 3. Time evolution of δ_m (see equation (7)) for the simulation before assimilation (solid line) and after assimilation (dashed line): (a) for the April campaign and (b) for the October campaign.

In all simulations, since the bias is on average small, there is very little difference between σ_m and the standard deviation (not shown).

The large initial value of σ_m in Figure 2b is due in part to the fact that the chemical fields in the CTM simulations were initialized from an earlier MOZART simulation performed with climatological winds [*Hauglustaine et al.*, 1998]. The initial geographical distribution of CO in the model compared poorly with the observations. The use of climatological winds is not the main source of discrepancy in this case since the modeled CO distribution lacked regions of high CO concentrations (not shown), regions that are present in the observations. Furthermore, a simulation starting 10 days before the first data are available for assimilation indicated very little difference with the results shown here.

4.2. Comparison With CMDL Observations

The Climate Monitoring and Diagnostics Laboratory (CMDL/NOAA) has compiled intercalibrated CO observations for the April and October period of 1994 [*Novelli et al.*, 1998]. In situ measurements at surface stations, flask, and aircraft data are available. More information can be found on the CMDL Web site (http://www.cmdl.noaa.gov). Because the CMDL data are data set independent from MAPS, it provides a means to evaluate the effect of the assimilation of MAPS data on the distribution of CO. For that purpose, the model results, output every hour, were interpolated to the exact location of the observations and then compared with the observations. Because we wanted to identify the accumulated role of assimilating CO, only the data within the last 5 days of the simulation were used. The correlation plots are shown in Figure 4. On each plot, the RMS error (as defined by (6), but for the case of local CO concentrations, not weighted averages) is also listed. The assimilation always improves the simulation of CO, except for the very limited set of flask data in October. The improvement is seen the most clearly in the aircraft data sampled for midtroposphere. This characteristic can be expected since it is the altitude range that contributes the most to the MAPS data. In both April and October, the average improvement is of the order of 30% for the data between 5 and 10 km. Since no information is available in the boundary layer from MAPS, the improvement of the surface data is more limited.

4.3. Amplitude of Adjustment

The process of assimilation results in an adjustment of the modeled CO field. The amplitude of such an adjustment is provided by the difference between the CO burden derived from model runs with and without assimilation. A positive (negative) value indicates that the assimilation acts as a source (sink) of CO. Figures 5a and 5b show the CO burden difference for the April and October cases, respectively. In both cases, it is clear that the largest adjustments occur in the beginning stages of the assimilation.

The early adjustments in the October case are particularly large, suggesting a significant underestimation of the impact of biomass burning sources of CO in the Southern Hemisphere. This points to an underestimation in the model either of the CO sources, or of the boundary layer venting associated with convection.

After substantial initial adjustments, the amplitude of adjustments decreases with time and oscillates around the zero line, suggesting that CO distributions were influenced by previous adjustments. Therefore, after a few cycles of assimilating CO, the assimilation seems to act primarily to redistribute CO. The time evolution of the adjustments would be smoother if the assimilation were performed more frequently than once every 12 hours, but without much impact on the overall results.

When integrated over the length of the simulation, the adjustments of the CO concentration added to the model CO burden 1.88 and 5.36 Tg-CO for the April and October cases, respectively. These numbers can be compared with an annual global surface emissions larger than 1200 Tg-CO [*Logan et al.*, 1981; *Müller and Brasseur*, 1995; *Berntsen and Isaksen*, 1997; *Hauglustaine et al.*, 1998; *Brasseur et al.*, 1999]. In particular, global CO emissions from biomass burning account on average for 300 to 900 Tg-CO/yr [*Brasseur et al.*, 1999, and references therein]. Assuming an emission of 500 Tg-CO/yr and 4 months of burning, the biomass burning source contributes of the order of 40 Tg-CO/yr in 10 days, indicating that the adjustment in the October case is of significant amplitude.

4.4. Lifetime of Adjustment

So far, we have analyzed the effect of assimilating the MAPS data over the entire period of observations. It is also interesting to estimate the time required for the CO to "forget" the state that results from the adjustment toward the observations. To that end, we designed an experiment in which we assimilated CO for the first day of the simulation (i.e., for two assimilation cycles), and then let the model drift freely, without assimilation. The evolution of σ_m (see equation (6)) for this case and for the case with assimilation provides an estimate of the adjustment lifetime. The difference in σ_m is shown for the April case in Figure 6. At first the difference is exactly 0 since both simulations were subject to the assimilation of CO. Then the difference grows quickly, until it reaches an almost constant value for the rest of the simulation. We expected that the difference in σ_m between the two simulations would be stable after an adjustment period because the value of σ_m after assimilation is almost constant with time (see Figures 2a and 2b). The results in Figure 6 show that the model CO field "memory" of its adjustment from the

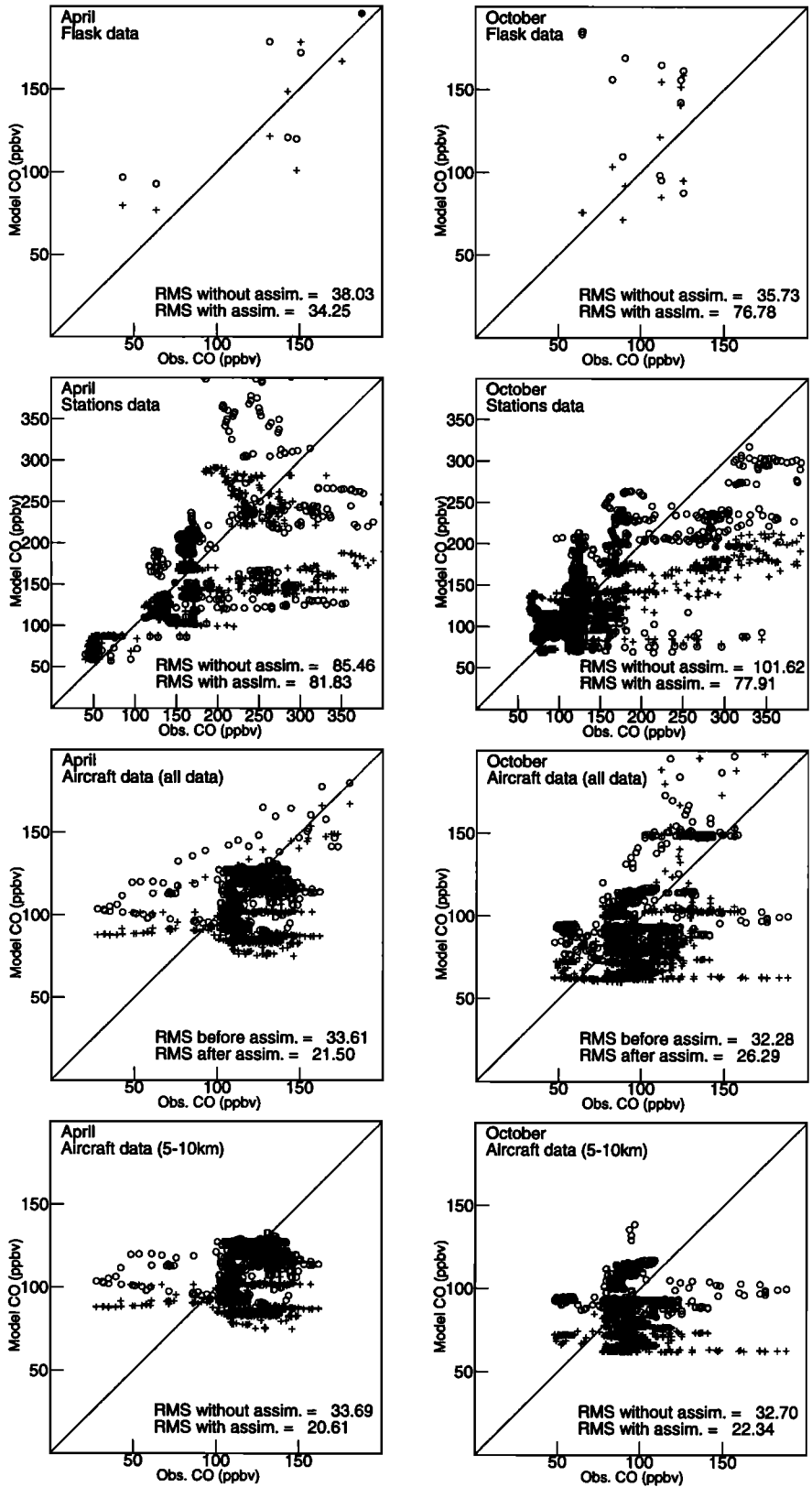

Figure 4. Comparison of model results with available CO observations [*Novelli et al.*, 1998] in April and October 1994. The data consist of flask data, in situ surface measurements, and aircraft measurements. The model results from the simulation with (without) assimilation are identified by open circles (pluses). The root-mean-square error (see text for details) is calculated for both simulations.

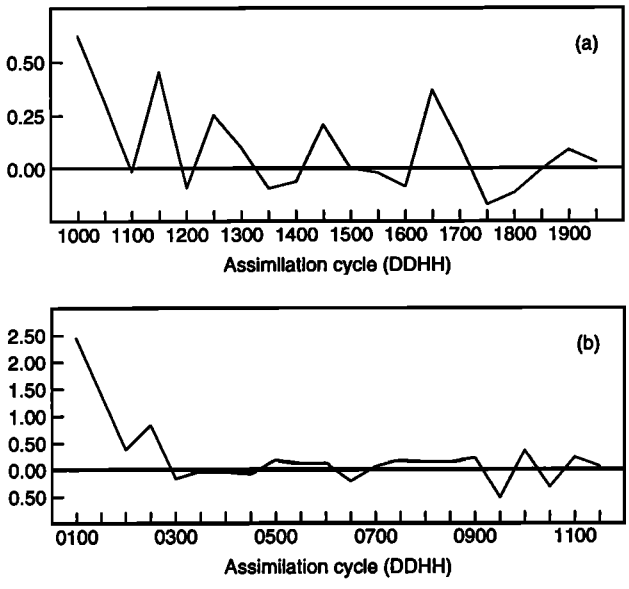

Figure 5. Time evolution of the difference in the burden of modeled CO from the assimilation, in Tg-CO. A positive value indicates that the assimilation has increased the amount of CO present in the model: (a) for the April campaign (time integrated total = 1.88 Tg-CO) and (b) for the October campaign (time integrated total = 5.36 Tg-CO).

assimilation is of the order of 1 to 2 days. Therefore, for this model setup, accurate assimilation of CO requires a coverage with gaps no longer than a few days. This adjustment lifetime is mostly related to errors in the redistribution of CO from errors associated with transport (see section 4.5). Since horizontal transport is layered vertically, errors in the vertical redistribution of the adjustment of CO will lead to errors in the subsequent transport of CO, even if the meteorology used for transport is correct.

4.5. Transport Versus Chemistry

In this section, we investigate the origin of the drift between model and observations over the 12-hour period between two consecutive assimilation cycles. Because only transport and chemistry (including surface sources) influence the CO distribution, the drift can only be due to errors in either one of these processes.

To examine the model drift, we compared the evolution of σ_m for two simulations of CO with assimilation: one with, and the other without chemical transformations. Chemical species sources were present in both simulations. As shown by Figure 7 for the April case, we found no significant difference between the two simulations, indicating that, over the 10-day period of study, the chemistry of CO did not play a significant role in the drift of the calculated distribution from the observations. The limited role of chemistry is of course related to the chemical lifetime of CO, estimated to be of the order of 2 months in the troposphere [*Hauglustaine et al.*, 1998]. Because chemistry was not an important factor over the period of study, reducing the full chemistry to a simple methane chemistry (see section 3.1) had very little influence. Nevertheless, chemistry's inclusion in the model allows us to assess the impact of CO assimilation on the distribution of other chemical species (see section 4.6).

4.6. Effect on Other Chemical Species

Because CO provides the major sink of OH in the free troposphere, a modification of the CO distribution associated with the assimilation procedure will directly affect the calculated OH distribution. To quantify this effect, we calculated the relative difference in the OH concentration between simulations with and without assimilation. In order to identify the accumulated effect, this difference is shown only at the end of the simulation. Because of the central role of ozone on tropospheric chemistry, we also analyzed the effect of CO assimilation on the distribution of ozone, using the same methodology as for OH.

Since the information contained in the MAPS data pertains mostly to the midtroposphere, the relative difference for CO, OH, and ozone are displayed for the 500 mbar level. This difference is calculated as the simulation with assimilation minus the simulation without assimilation. A positive (negative) value indicates an increase (decrease) in the concentration of CO resulting from its assimilation. These differences show the effect of the assimilation procedure on chemical species. They do not represent the effect of sources (biomass burning in particular) on the tropospheric ozone distribution [e.g., *Fishman and Brackett*, 1997].

In the April case (Plates 2a-2c), there are localized effects on OH of the order of 30%, both positive and negative. Not much significant difference, however, can be found in the case of ozone. This difference is consistent with the fact that CO is significantly modified only over a limited number of regions.

In the October case (Plates 2d-2f), large portions of the Southern Hemisphere are characterized by a decrease in OH greater than 30%. The changes are associated with regions where the CO concentrations were significantly increased in response to the assimilation, and over the Indian Ocean in particular, where the increase of CO is of the order of 300%. As mentioned in

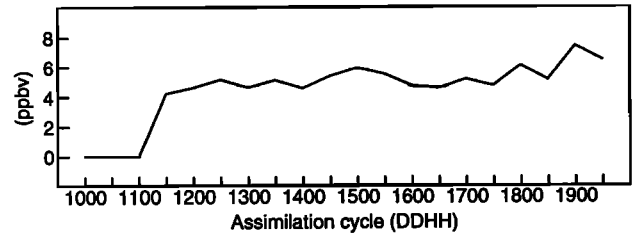

Figure 6. Time evolution of the difference in σ_m (see equation (6)) between the simulation with continuous assimilation and the simulation with assimilation during the first day.

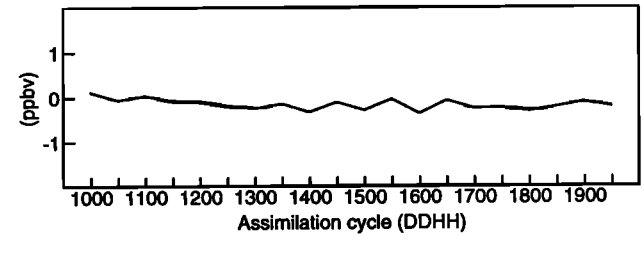

Figure 7. Time evolution of the difference in σ_m (see equation (6)) between the simulation with chemistry and the simulation without chemistry. In both cases, the assimilation of CO is performed.

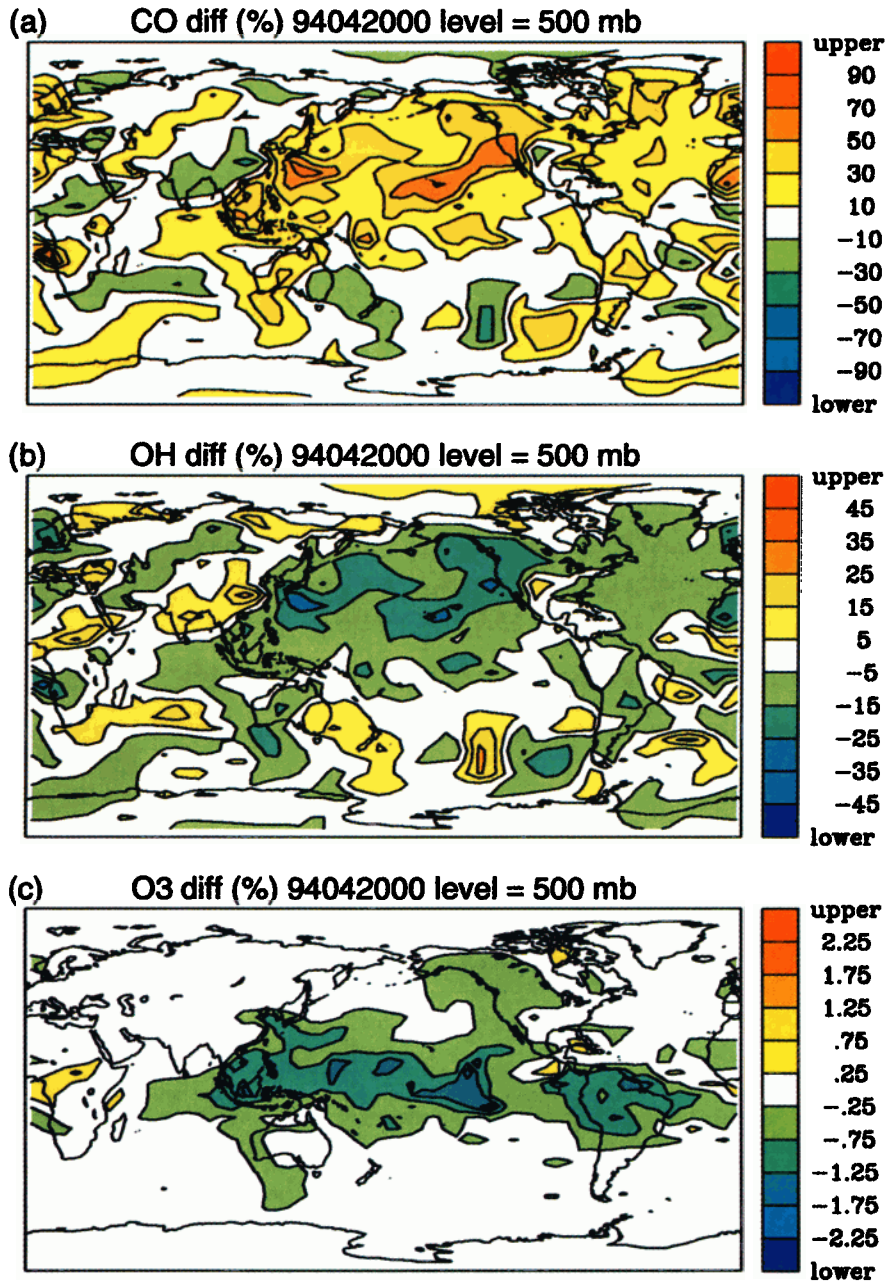

Plate 2. Latitude-longitude distribution at 500 mbar of the relative difference (percent) between the simulation with assimilation and the simulation without assimilation. A positive value indicates an increase of the considered species due to the assimilation of CO. (a) For CO in April, (b) for OH in April, (c) for O_3 in April, (d) for CO in October, (e) for OH in October, and (f) for O_3 in October.

section 4.2, this increase in the abundance of CO is probably related to an underestimation of the biomass burning sources in MOZART over Africa, Southeast Asia, and South America and/or the boundary layer venting over those regions. Owing to its short lifetime, the OH perturbation is everywhere collocated with the CO perturbation. This collocation indicates that the free troposphere is in a chemical regime where NO_x ($NO + NO_2$), not CO is the rate-limiting precursor of ozone production. If the free troposphere were CO-limited, then a CO increase would imply an increase in both OH and ozone [*Hess and Madronich*, 1997]. The large OH perturbation is associated with a negative perturbation in ozone that is larger than 6% over the Indian Ocean. Owing to the longer lifetime of ozone, this feature spreads downwind from the maximum OH perturbation. The same analysis applies to the ozone perturbation at the northern tip of South America. All chemical species are therefore affected by the assimilation of CO, to a degree that is dependent on the chemical coupling of these species with CO.

5. Discussion and Conclusions

In this study we have performed a successful assimilation of the MAPS observations of CO into the global three-dimensional chemistry-transport model named MOZART. Every 12 hours, the MAPS data accumulated over the previous 12 hours provide

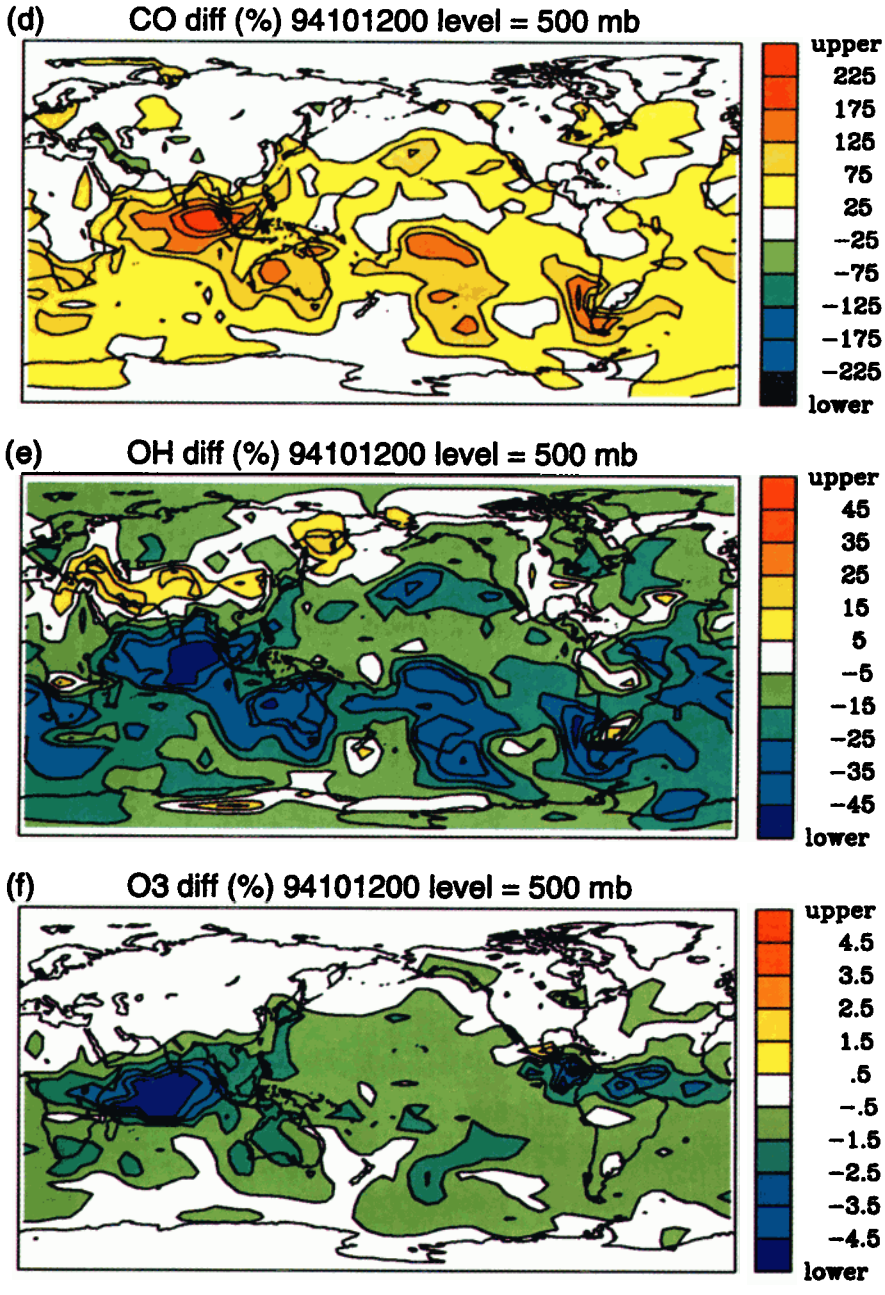

Plate 2. (continued)

a latitudinally and longitudinally extensive coverage of a measure of tropospheric CO, with an emphasis on the midtroposphere. Owing to the shape of the MAPS instrument signal function, the data do not provide information on the concentration of CO in the boundary layer.

When the MAPS data were assimilated into the MOZART model, the calculated CO fields improved significantly. The improvement clearly pertains to the value obtained after the convolution of the model CO with the MAPS averaging kernel (Figure 1). Also, comparison of the model results with available data at the surface and in the troposphere indicate that, on average, the assimilation of MAPS data improves the simulation of CO. The improvement is the most significant in the free troposphere. At the surface, since the averaging kernel is close to 0 in the boundary layer, the simulated CO is little modified by the assimilation scheme. As a consequence, only limited improvement can be achieved in that portion of the troposphere.

Comparison of the geographical distribution of the adjustments of CO toward the observations suggests a misrepresentation of the amplitude of the biomass burning source of CO in the model. This is consistent with previous model analysis [*Hauglustaine et al.*, 1998] and observations [*Nichol*, 1998]. This identifies data assimilation as a possible method to quantify the amplitude and location of CO sources.

Because the amplitude of the adjustments that resulted from the assimilation of CO decreased over the course of the simulation, we can conclude that the modeled CO field has a limited "memory" of previous adjustments, estimated to be of the order of 1 to 2 days.

Transport seemed to be the primary contributor to the drift in CO between model and observations over the 12-hour period between subsequent assimilation cycles, and consequently to the limited adjustment "memory". This does not imply that transport was responsible for the discrepancy, since most of the difference

between model and observations was associated with the initial conditions of the simulations.

By the end of the October case simulation, the assimilation of CO led to a 6% change in ozone and 50% in OH over local regions. Changes of this magnitude suggest that assimilation of a single compound such as CO has a substantial influence on the calculated concentration of other chemical species in the troposphere.

The relatively short periods of available data and the lack of information from within the boundary layer limited our study. A large-scale, high-resolution, and long-term data set such as MOPITT (Measurement Of Pollution In The Troposphere, to be launched in 1999 as part of the Terra platform [*Drummond*, 1992]) will provide the necessary coverage to analyze and better constrain the budget of CO. Using the methodology presented in this paper, it will bring considerable insight into global tropospheric chemistry and the ability of models to reproduce the observed distributions of chemical species.

Acknowledgments. We wish to acknowledge P. Hess, E. Holland, W. Randel, and A. Bokman for their input on an earlier version of this paper. The authors are grateful to D. Hauglustaine for his valuable insights and assistance with MOZART. We are indebted to H. Reichle and V. Connors for allowing us access to the MAPS data. Discussions with R. Ménard have also greatly influenced the approach followed in this study. This work was supported by the NASA Earth Observing System (EOS) Program. The National Center for Atmospheric Research is operated by the University Corporation for Atmospheric Research under sponsorship of the National Science Foundation.

References

Allen, D. J., et al., Transport-induced interannual variability of carbon monoxide using a chemistry and transport model, *J. Geophys. Res.*, *101*, 28,655-28,669, 1996.

Berntsen, T. K., and I.S.A. Isaksen, A global three-dimensional chemical transport model for the troposphere, 1, Model description and CO and ozone results, *J. Geophys. Res.*, *102*, 21,239-21280, 1997.

Brasseur, G. P., D. A. Hauglustaine, S. Walters, P. J. Rasch, J.-F. Müller, C. Granier, and X. X. Tie, MOZART: A global chemical transport model for ozone and related chemical tracers, 1, Model description. *J. Geophys. Res.*, *103*, 28,265-28,290, 1998.

Brasseur, G. P., et al., Trace gas exchanges and biogeochemical cycles, in *Atmospheric Chemistry and Global Change*, edited by G. P. Brasseur, J. J. Orlando, and G. S. Tyndall, pp. 159-203, Oxford Univ. Press, New York, 1999.

Chatfield R. B., J.A., Vastano, L. Li, G. W. Sachse, and V. S. Connors, The Great African plume from biomass burning: Generalizations from a three-dimensional study of TRACE-A carbon monoxide, *J. Geophys. Res.*, *103*, 28,059-28,077, 1998.

Cohn, S.E., An introduction to estimation theory, *J. Meteorol. Soc. Jpn.*, *75*, 257-288, 1997.

Connors, V.S., M. Flood, T. Jones, B. Gormsen, S. Nolf, and H.G. Reichle Jr., Global distribution of biomass burning and carbon monoxide in the middle troposphere during early April and October 1994, in *Biomass Burning and Global Change*, edited by J. S. Levine, pp. 99-106, MIT Press, Cambridge, Mass., 1996.

Courtier, P., E. Andersson, W. Heckley, J. Pailleux, D. Vasiljevic, M. Hamrud, A. Hollingsworth, F. Rabier, and M. Fisher, The ECMWF implementation of three-dimension variational assimilation (3D-Var), I, Formulation, *Q. J. R. Meteorol. Soc.*, *124*, 1783-1807, 1998.

Crutzen, P., A discussion of the chemistry of some minor constituents in the stratosphere and troposphere, *Pure Appl. Geophys.*, *106-108*, 1385-1399, 1973.

Da Silva, A., and J. Guo, Documentation of the Physical-space Statistical Analysis System (PSAS), I, The conjugate gradient solver, *Office Note 96-02*, NASA, Washington, DC, 1996.

Da Silva, A., J. Pfaendtner, J. Guo, M. Siemkiewicz, and S. Cohn, Assessing the effects of data selection with DAO's Physical-space Statistical Analysis System, Proceedings of the Second International WMO Symposium on Assimilation of Observations in Meteorology and Oceanography, *WMO/TD 651*, World Meteorol. Org., Geneva, 1995.

Drummond, J. R., Measurements of Pollution in the Troposphere (MOPITT), *The Use of EOS for Studies of Atmospheric Physics*, Edited by J. Gille and G. Visconti, pp. 77-101, North Holland, New York, 1992.

Errico, R. M., Workshop on the assimilation of satellite data., *Bull. Am. Meteorol. Soc.*,. *80*, 463-471, 1999.

Fishman, J., and V. G. Brackett, The climatological distribution of tropospheric ozone derived from satellite measurements using version 7 Total Ozone Mapping Spectrometer and Stratospheric Aerosol and Gas Experiment data sets, *J. Geophys. Res.*, *102*, 19,275-19,278, 1997.

Gaspari, G., and S. E. Cohn, Construction of correlation functions in two and three dimensions, *Q. J. R. Meteorol. Soc.*, *125*, 723-757, 1999.

Hauglustaine, D. A., G. P. Brasseur, S. Walters, P. J. Rasch, J.-F. Müller, L. K. Emmons, and M. A. Carroll, MOZART: A global chemical transport model for ozone and related chemical tracers, 2, Model results and evaluation, *J. Geophys. Res.*, *103*, 28,291-28,336, 1998.

Hess, P.G. and S. Madronich, On tropospheric chemical oscillations, *J. Geophys. Res.*, *102*, 15,949-15,965, 1997.

Levy II, H., Normal atmosphere: large radical and formaldehyde concentrations predicted, *Science*, *173*, 141-143, 1971.

Logan, J. A., M. J. Prather, S. C. Wofsy, and M. B. McElroy, Tropospheric chemistry: A global perspective, *J. Geophys. Res.*, *86*, 7210-7254, 1981.

Lorenc, A. C., Analysis method for numerical weather prediction, *Q. J. R. Meteorol. Soc.*, *112*, 1177-1194, 1986.

Mahowald, N., P. Rasch, B. Eaton, S. Whittleston, and R. Prinn, Transport of ^{222}Rn to the remote troposphere using MATCH and assimilated winds from ECMWF and NCEP/NCAR, *J. Geophys. Res.*, *102*, 28,139-28,151, 1997.

Müller, J.-F., and G.P. Brasseur, IMAGES: A three-dimensional chemical transport model of the global troposphere, *J. Geophys. Res.*, *100*, 16445-16490, 1995.

Nichol, J., Bioclimatic impacts of the 1994 smoke haze event in Southeast Asia, *Atmos. Environment*, *32*, 2715-2716, 1998.

Novelli, P. C., et al., An internally consistent set of globally distributed atmospheric carbon monoxide mixing rations developed using results from an intercomparison of measurements, *J. Geophys. Res.*, *103*, 19,285-19,293, 1998.

Rasch, P. J., N. M. Mahowald, and B. E. Eaton, Representation of transport, convection, and the hydrological cycle in chemical transport models: Implications for the modeling of short lived and soluble species, *J. Geophys. Res.*, *102*, 28,127-28,138, 1997.

Reichle, H. G., V. S. Connors, J. A. Holland, R. T. Sherrill, H. A. Wallio, J. C. Casas, E. P. Condon, B. B. Gormsen, and W. Seiler, The distribution of middle tropospheric carbon monoxide during early October 1984, *J. Geophys. Res.*, *95*, 9,845-9,856, 1990.

Reichle, H. G., et al., Space shuttle based global CO measurements during April and October 1994, MAPS instrument, data reduction, and data validation, *J. Geophys. Res.*, in press, 1999.

Talagrand, O., Assimilation of observations, an Introduction, *J. Meteorol. Soc. of Jpn.*, *75*, 191-209, 1997.

G. P. Brasseur, J. C. Gille, B. V. Khattatov, and J.-F. Lamarque, NCAR/ACD, P.O. Box 3000, Boulder, CO 80307-3000. (brasseur@ucar.edu; gille@ucar.edu; boris@ucar.edu; lamar@ucar.edu)

(Received January 25, 1999; revised July 19, 1999; accepted July 26, 1999.)